Applied Catalysis B: Environmental 136–137 (2013) 269–277

Contents lists available at SciVerse ScienceDirect

Applied Catalysis B: Environmental

journal homepage: www.elsevier.com/locate/apcatb

Well-dispersed g-C_3N_4 nanophases in mesoporous silica channels and their catalytic activity for carbon dioxide activation and conversion

Zhijun Huang[a,b], Fengbo Li[a,*], Bingfeng Chen[a,b], Tao Lu[a,b], Yin Yuan[a,b], Guoqing Yuan[a,*]

[a] Beijing National Laboratory of Molecular Science, Laboratory of New Materials Institute of Chemistry, Chinese Academy of Sciences, Beijing, PR China
[b] University of Chinese Academy of Sciences, Beijing, 100049, PR China

ARTICLE INFO

Article history:
Received 30 July 2012
Received in revised form 28 January 2013
Accepted 29 January 2013
Available online 14 February 2013

Keywords:
Heterogeneous catalysis
Carbides
Nanomaterials
Fixation of carbon dioxide
Cycloaddition

ABSTRACT

Well-dispersed g-C_3N_4 nanophases in SBA-15 mesochannels were prepared by a two-step vapor condensation of dicyandiamide. Defect-containing g-C_3N_4 nanophases were active catalysts for CO_2 activation. Activated CO_2 species were steadily converted to target compounds with a high selectivity. The presence of doped metal ions markedly promoted the catalytic activity and selectivity. Zn^{2+}-doped g-C_3N_4/SBA-15 showed a high activity in transferring CO_2 to epoxides. Fe^{3+}-doped g-C_3N_4/SBA-15 was an efficient catalyst for the direct oxidative cycloadditon of CO_2 to olefins. Styrene was converted into 4-phenyl-1, 3-dioxolan-2-one. The process conversion was 34.1% and the selectivity to the oxidative cycloaddition product reached 93%. The recyclability of SBA-15 supported g-C_3N_4 nanophases was investigated through a five-run test. Their catalytic activity and microstructures were kept constant during the five-run recycling test. No marked metal leaching was detected during each test.

1. Introduction

Energy is a central topic in the modern society economy. Fossil fuel provides 81% of the world's commercial energy supply [1] and releases nearly 30 Pg (pentagram) of carbon dioxide annually from the permanent and stable carbon pools to the mobile carbon pools on earth. The deviation from equilibrium has caused severe environmental concerns such as global warming, the eutrophication of terrestrial and oceanic ecosystems, and the acidification of the ocean [2–5]. Practical solutions for managing anthropogenic carbon are to stop or reverse the build-up of CO_2 in the environment. Unfortunately, economic and population growth makes it difficult to abate or replace the use of fossil fuels. There are two practical solutions: to capture and store anthropogenic carbon [6] and to use CO_2 as a starting carbon feedstock for basic chemicals [7].

Carbon dioxide is the most stable form of carbon ($\Delta_f G_{298}^\circ = -394.36$ kJ/mol). When CO_2 is used as a chemical feedstock, its activation is the key step. Large amounts of carbon dioxide are utilized in the reaction with ammonia for the synthesis of urea and in the reactions with phenolates (Kolbe–Schmitt synthesis) for producing salicylic acids. Most reactions of CO_2 require activation by metals or metal complexes. These reactions include the synthesis of organic carbonates and polycarbonates and the hydrogenation of CO_2 to methanol or formic acid. Grignard carboxylations and electrochemical reactions with reactive anodes (Al, Mg) can activate carbon dioxide, but produce waste in an equivalent amount of the desired products. Enzymatic CO_2 activation is complex in their natural processes and far from the practical synthetic systems. Because of the importance of practical carbon dioxide utilization, extensive book chapters and reviews have covered the above-listed topics [8–13]. Recently, some sustainable catalytic processes were harnessed to convert CO_2, such as photoreduction of CO_2 [14–16], low-temperature catalytic reduction of CO_2 with hydrogen [17], electrochemical reduction of CO_2 [18], and novel catalytic coupling of epoxides and CO_2 [19,20]. CO_2 has been proven to be a soft oxidant for some organic synthesis [21].

In this work, we report the activation and conversion of CO_2 over supported g-C_3N_4 nanophases under relatively mild conditions. Carbon dioxide interacts easily with several N-nucleophiles through either ironically or covalently bonding to the electrophilic centers [22–25]. The formation of N-carbonyl plays a key role in the development of these sustainable conversions. Unfortunately, the large-amount use of N-nucleophile makes these processes only valuable in the laboratory scale. There is a quest for more eco-friendly reusable heterogeneous catalysts that are capable of promoting the fixation of the carbon dioxide with high yield and selectivity under as much as possible mild conditions. Polymeric graphitic carbon nitride materials (for simplicity: g-C_3N_4) is nitrogen-rich carbon nitride [26–31]. Theoretical study predicts many unusual properties [32]. These materials are promising heterogeneous catalysts for CO_2 activation. Through replacing carbon with nitrogen in graphite with various ways, carbon

* Corresponding authors. Fax: +86 10 62559373.
E-mail addresses: lifb@iccas.ac.cn (F. Li), yuangq@iccas.ac.cn (G. Yuan).

0926-3373/$ – see front matter © 2013 Elsevier B.V. All rights reserved.
http://dx.doi.org/10.1016/j.apcatb.2013.01.057

nitride exhibits various possibilities in building up lattice with exciting new properties [33]. Carbon nitride generally shows a high thermal and chemical stability and an electronic structure suitable for catalyzing many chemical reactions. Graphitic-C_3N_4 and some incompletely condensed precursors have shown promising applications in heterogeneous metal-free catalysts [34–37], photocatalysts [38–40], and catalytic active sites' supports [41,42]. To enhance the catalytic performance, mesostructured gaphitic-C_3N_4 was synthesized through hard templating methods [43,44]. The synthesis of g-C_3N_4 generally involves the pyrolysis of nitrogen-rich precursors, which incorporates the condensation and polymerization of triazine rings [45–47].

2. Experimental

2.1. Materials

Dicyandiamide, tetraethylorthosilicate (TEOS), styrene oxide, propylene oxide, ethylene oxide, acetonitrile, and olefins were purchased from Sinopharm Chemical Reagent Co. Ltd. P123 (Pluronic P123, BASF) was purchased from Aldrich. Acetonitrile was distilled before using. Metal acetylacetonate salts were purchased from Strem. All the reagents were used as received.

2.2. SBA-15

Triblock copolymer (Pluronic P123, BASF, 4.0 g) was dissolved overnight in 105 ml of water (500-ml beaker) under stirring. The solution was heated to 35 °C and stirred for 30 min after 20 ml of HCl (37%) was added. TEOS (8.5 g) was added dropwise under vigorous stirring. The mixture was stirred for further 4 h. The white solid was collected by filtration and washed with deionized water to remove the excess triblock copolymer template and acid. The resulting solid materials were dried at 80 °C in air and then heated to 550 °C with a temperature increasing rate of 1 °C/min. SBA-15 was obtained after further 5-h calcining in air.

2.3. Graphitic C_3N_4/SBA-15

Graphitic C_3N_4/SBA-15 was prepared with a program-controlled furnace. Dicyandiamide (2.0 g) was placed in a quartz boat and SBA-15 (1.0 g) was placed in the next quartz boat. The preparation equipment was flushed with argon for 30 min. The temperature was increased to 230 °C in 30 min and kept for 3 h. Dicyandiamide's boiling point is 229.8 °C at 760 mmHg. Argon was used as a carrier gas and the Ar flow rate was in the range of 10–100 ml/min. The operating pressure was approximately 1.0 atm. In the following procedure, the treatment temperature was increased to 450 °C in 30 min and kept for 1 h. Graphitic-C_3N_4/SBA-15 with different load amount and dispersion states could be synthesized by controlling the reaction time and the Ar flow rate. The loaded samples were treated at 600 °C for further 4 h. Graphitic-C_3N_4/SBA-15 (carbon nitride load: 5.3 wt%) was obtained at 230 °C for 3 h under the Ar flow of 20 ml/min. Carbon nitrides over MCM-41 were prepared by the same procedure by replacing SBA-15 with MCM-41.

Mesoporous carbon nitrides were prepared by using SBA-15 as the hard template. SBA-15 (1.0 g) was impregnated with an aqueous solution of dicyandiamine. The sample was dried in air at 90 °C. The dried mixture was treated at 450 °C for further 3 h and at 600 °C for 1 h in the argon flow of 30 ml/min. Hard template (SBA-15) was removed by suspending the solid materials in HF aqueous solution (10%) under vigorous stirring for 24 h in a polyethylene bottle.

2.4. Zn-doped g-C_3N_4/SBA-15

Graphitic-C_3N_4/SBA-15 (0.1 g) was suspended in CH_3CN solution of Zn $(acac)_2$ (10 ml, 0.1 M). The mixture was stirred at room temperature for 24 h and filtered. The solid was washed by CH_3CN for five times and dried under vacuum for 12 h. The sample was calcined in air for 5 h at 650 °C, and digested by HF solution. The Zn concentration was determined by inductively coupled plasma atomic emission spectroscopy (ICP-OES) by using PerkinElmer Optima 5300 dv. Other transition metal ions doped g-C_3N_4/SBA-15 materials were prepared by the same procedure with the CH_3CN solution containing corresponding metal acetylacetonate salts.

2.5. Catalytic activity test

Transferring CO_2 to epoxides: the catalytic tests were carried out in a 50-ml autoclave with the inner-Teflon coat. Typical reaction conditions: styrene oxide (3.0 ml), reaction temperature (150 °C), CO_2 pressure (3.5 MPa), reaction time (1.5 h), the catalyst amount (0.1 g).

Direct oxidative cycloadditon of CO_2 to olefins: The catalytic test was carried out in a 50-ml autoclave with the inner-Teflon coat. Typical reaction conditions: olefin (3.0 mmol), 1, 4-dioxane (3.0 ml), reaction temperature (150 °C), CO_2 pressure (3.5 MPa), reaction time (5 h), catalyst amount (0.1 g).

Oxygen-aided oxidative cycloadditon of CO_2 to olefins: The catalytic test was carried out in a 50-ml autoclave with the inner-Teflon coat. Typical reaction conditions: olefin (3.0 mmol), 1, 4-dioxane (3.0 ml), reaction temperature (150 °C), CO_2 pressure (3.0 MPa), oxygen pressure (0.5 MPa), reaction time (5 h), catalyst amount (0.1 g).

2.6. Characterization and methods

Elemental analysis was performed on a Flash EA 1112. Powder XRD patterns were measured on a Rigaku Rotaflex diffractometer equipped with a rotating anode and a Cu Kα radiation source (40 kV, 200 mA; λ = 1.54056 Å). XPS data were obtained with an ESCALab220i-XL electron spectrometer from VG Scientific using 300 W Al Kα radiations. The base pressure was approximately 3×10^{-9} mbar. The binding energies were referenced to the C1s line at 284.8 eV from adventitious carbon. The Eclipse V2.1 data analysis software supplied by the VG ESCA-Lab200I-XL instrument manufacturer was used to manipulate the acquired spectra. Nitrogen adsorption isothermal and textural properties of the as-synthesized materials were determined at 77.3 K using nitrogen by a Quantachrome Autosorb Automated Gas Sorption System (Quantachrome Corporation). Before analysis, all samples were dried at 300 °C under vacuum for 6 h. Transmission electron microscopy (TEM) was performed on a JEOL 2010 TEM operated at an accelerating voltage of 200 kV. Reaction products were analyzed by GC and GC–MS. GC was performed on a GC-2014 (SHIMADZU) equipped with a high temperature capillary column (MXT-1, 30 m, 0.25 mm ID) and a FID detector. GC-MS was performed on a GCT Premier/Waters equipped with a capillary column (DB-5MS/J&W Scientific, 30 m, 0.25 mm ID).

3. Results and discussion

3.1. Dispersion of g-C_3N_4 nanophases in silica mesochannels

Carbon nitride nanophases in SBA-15 channels were introduced through a two-step condensation method (Scheme 1). TEM characterization gives a clear view of the dispersion state of g-C_3N_4. SBA-15, prepared by a well-established method [48], has highly ordered mesostructures (Fig. 1a). Its pore width is about 8.26 nm. Carbon nitride nanophases are located over the pore walls with the

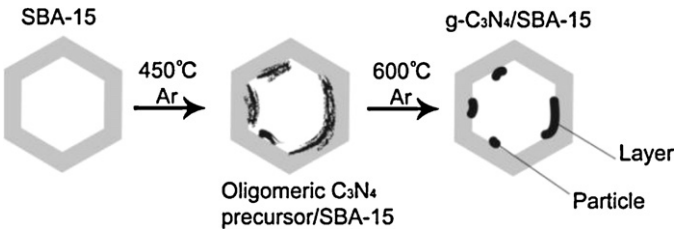

Scheme 1. Illustration of the two-step vapor condensation for preparing well-dispersed g-C_3N_4 nanophases in SBA-15 channels.

load amount of 5.3 wt% (Fig. 1b). Fig. 1c is the TEM image of the as-synthesized sample from face 1 1 0. The small-angle powder XRD pattern (Fig. 1d) of the sample depicted in Fig. 1b exhibits three typical peaks of SBA-15 (1 0 0, 1 1 0, 2 0 0) [48]. The introducing of g-C_3N_4 nanophases has not changed the pore structure of SBA-15.

Recent works have demonstrated that the pyrolysis of dicyandiamide yields a melon polymer built up from melem units (Fig. 2a) [49,50]. This tecton is the most energetically favored building unit for g-C_3N_4. The tri-s-triazine rings are cross-linked by trigonal nitrogen atoms to form condensed, crystalline C_3N_4 phase. However, it remains a great challenge to synthesize perfect crystalline C_3N_4 phase. The bulk synthesis methods indeed lead to C/N/H-containing polymeric compounds. The C/N molar ratio of the supported carbon nitride can be detected by elemental analysis. This parameter is an important index to the structural integrity of the carbon nitride. As shown in Fig. 2a, the theoretical C/N molar ratio of a local unit is calculated based on the molecular model (C/N ratio = $6/(7+f_x+f_y+f_z)$) of tri-s-triazine ring and cross-linked trigonal nitrogen atoms [51–53]. f_x, f_y, and f_z are the fraction coefficients of each trigonal nitrogen atom to the tri-s-triazine ring. When f_x, f_y, and f_z are totally equal to 1, the molecular structure is a single melem. There is no cross-linking among the tri-s-triazines and the calculated C/N ratio is 0.6. When f_x, f_y, and f_z are totally equal to 1/3, trigonal cross-linked nitrogen atoms are fully occupied, and the molecular structure is an ideal crystalline C_3N_4 phase. The calculated C/N molar ratio is 0.75 for a perfect g-C_3N_4. The measured C/N molar ratio of the as-synthesized carbon nitride is a statistical value from all local units with various degrees of cross-linking. The value is in the range from 0.60 to 0.75. The bigger the measured C/N molar ratio is, the higher the degree of cross-linking is. In the first step of the two-step condensation process, oligomeric C_xN_y precursors were introduced the inner walls of the mesochannels. Further treatment at 600 °C deeply polymerized these oligomeric precursors to form g-C_3N_4. The measured C/N molar ratio of supported carbon nitride nanophases increases with the thermal treatment time at 600 °C (Fig. 2b). After 3.0 h of treatment, the measured C/N molar ratio shows slight changes. The as-synthesized materials have the measured C/N molar ratio of approximately 0.74. The supported carbon nitride nanophases are defect-containing, polymeric g-C_3N_4, which are far more active than perfectly crystalline g-C_3N_4.

Fig. 3 shows N_2 adsorption-desorption isotherms of SBA-15 and g-C_3N_4/SBA-15. Pure SBA-15 has a BET surface area of 512 m^2/g. That of g-C_3N_4/SBA-15 is 586 m^2/g. The presence of g-C_3N_4

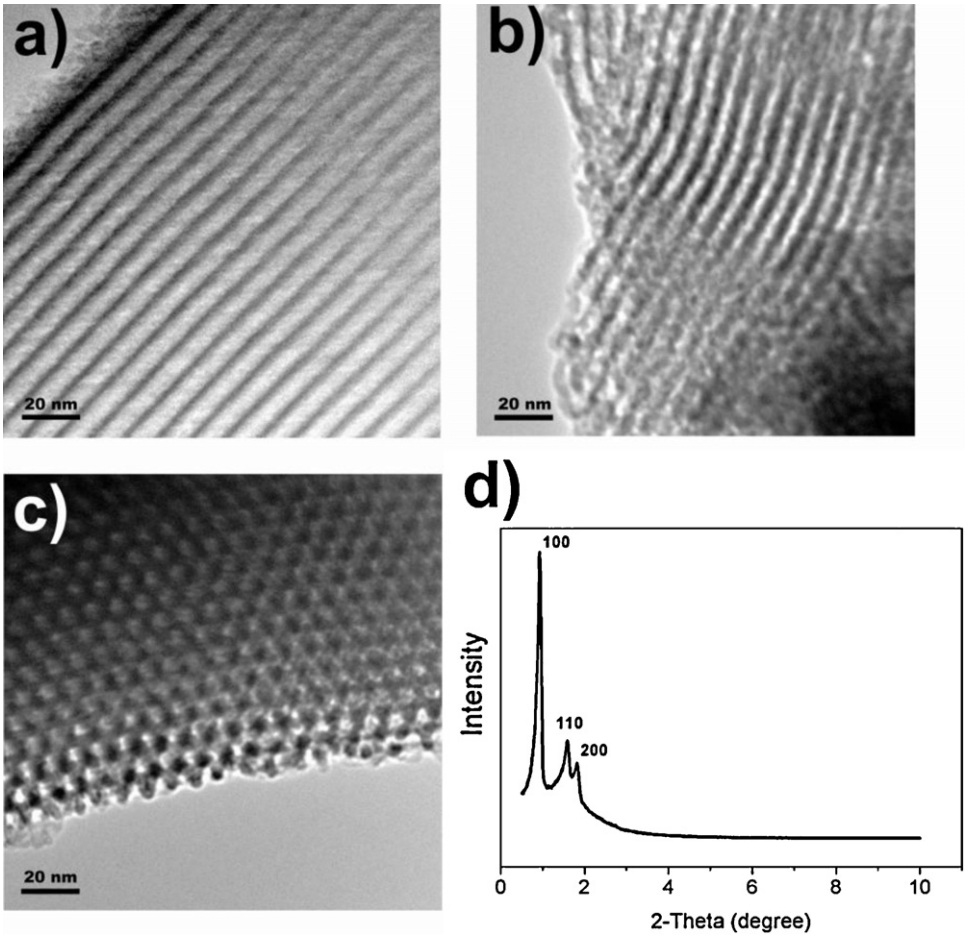

Fig. 1. (a) TEM image of SBA-15 (face 1 0 0). (b) TEM image of g-C_3N_4 in SBA-15 mesochannels (face 1 0 0). (c) TEM image of g-C_3N_4 in SBA-15 mesochannels (face 1 1 0). (d) Small-angle powder X-ray diffraction pattern of g-C_3N_4/SBA-15.

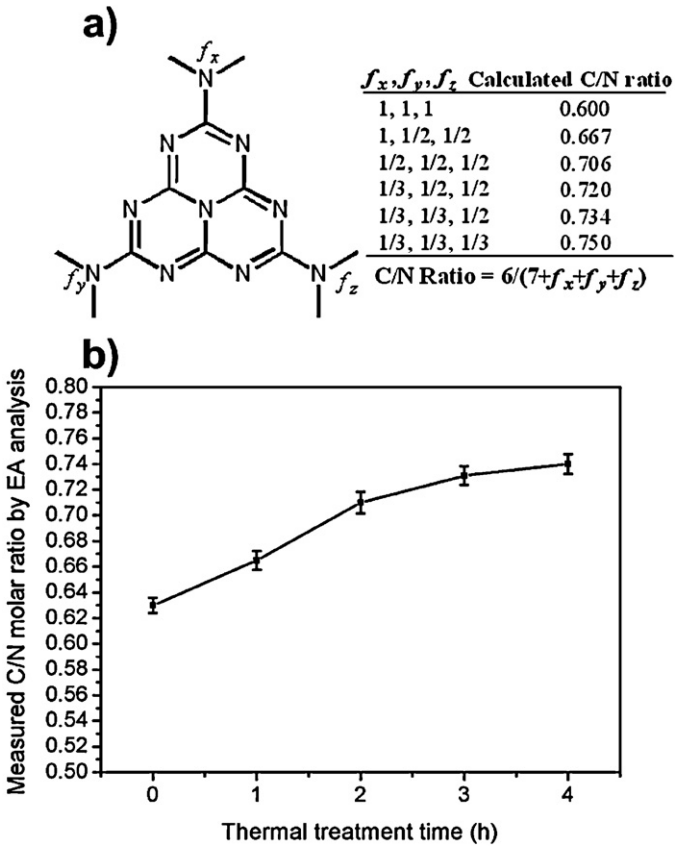

Fig. 2. (a) Molecular model for theoretical C/N molar ratio calculation of polymeric melem structures. (b) The measured C/N molar ratio of supported carbon nitride nanophases under different thermal treatment times at 600 °C.

nanophases causes a decrease of pore width from 8.26 nm to 6.61 nm (the insert of Fig. 3). The hysteresis loops of the N_2 adsorption-desorption isotherms (Fig. 3) are Type H1 [54], which indicates regular even pores without interconnecting channels. Compared to the N_2 adsorption-desorption isotherm of SBA-15 (Fig. 3A), the hysteresis loop of g-C_3N_4/SBA-15 (Fig. 3B) appears to be broadened. The pore uniformity is lowered and this is confirmed by Fig. 1b. Carbon nitride nanophases contain various amorphousness and dislocation, which add sub-structures to the silica pore matrix and lead to the increase in the BET surface area of g-C_3N_4/SBA-15. The incipient wet impregnation suffers a

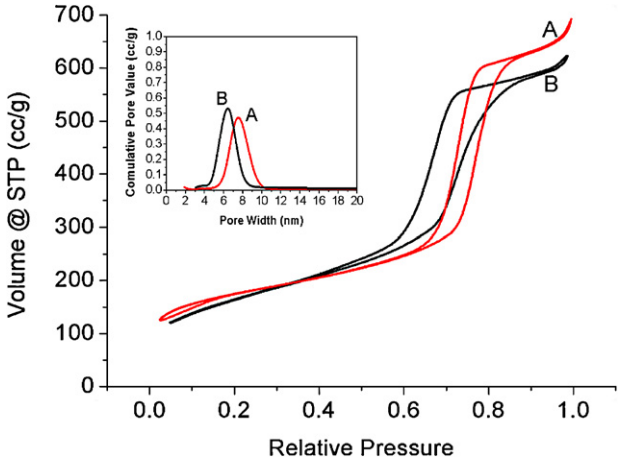

Fig. 3. N_2 adsorption–desorption isotherm of SBA-15 (A) and g-C_3N_4/SBA-15 (B). The insert is the BJH pore distribution of SBA-15 (A) and g-C_3N_4/SBA-15 (B).

Table 1
Porosity properties of silica supports and the resulting composites.

Sample	S_{BET} (m^2/g)	Pore diameter (nm)	Pore volume ($cm^3\ g^{-1}$)
SBA-15	512	8.26	0.940
g-C_3N_4/SBA-15	586	6.61	0.939
g-C_3N_4/SBA-15[a]	315	7.87	0.623
MCM-41	1092	2.81	0.893
g-C_3N_4/MCM-41	224	1.35	0.267
Porous g-C_3N_4[b]	632	4.01	1.03
g-C_3N_4	2	–	–
Zn-g-C_3N_4/SBA-15	585	6.53	0.928
Fe-g-C_3N_4/SBA-15	586	6.59	0.931

[a] The sample was prepared by the incipient wet impregnation of the precursors.
[b] SBA-15 was used the hard template and the silica structures were removed by HF aqueous solution.

drawback in that capillary forces take up the liquid into the pore system and lead to the deposition of active precursor at the external edges of the pores during drying the wet sample. This effect encloses the pores and lowers the apparent surface area. Carbon nitrides supported over SBA-15, prepared by the wet impregnation, show a marked decrease in the surface area (Table 1). The vapor-phase deposition causes blocking of MCM-41's pore system with the narrower pore width of 2.81 nm. The materials lose most of the surface areas. Mesoporous g-C_3N_4 prepared by using SBA-15 as the hard template has better porosity properties than that of g-C_3N_4/SBA-15 (Table 1). Doping of transition metal ions has negligible effects on the porosity properies.

XPS characterization of SBA-15 supported g-C_3N_4 and bulk g-C_3N_4 was performed to investigate size-dependent phenomena of the supported nanophases [44]. As revealed by the C1s and N1s XPS peaks, there were marked differences in the electronic structure between the supported g-C_3N_4 and the bulk g-C_3N_4 (Fig. 4). Fitting of the C1s envelope resulted in the identification of two chemical states of carbon (Fig. 4a). For the bulk g-C_3N_4 (B), the main carbon chemical state was the C1s peak at the binding energy of 288.1 eV, which was attributed to tri-s-triazine. However, the main carbon chemical state of SBA-15 supported g-C_3N_4 nanophases was the C1s peak at the binding energy of 284.7 eV (A), which was close to the carbon chemical state of graphite. Fitting of the N1s envelope resulted in the identification of two chemical states of nitrogen (Fig. 4b) in a tri-s-triazine unit. The mole ratios of two nitrogen chemical states were 7.63:2.37 for the bulk g-C_3N_4 and 7.47:2.53 for the supported g-C_3N_4. These values were close to the theoretical value (7:3) of an ideal g-C_3N_4 structure. The C1s XPS peaks were selected as the indicator of the electronic structure of g-C_3N_4. A shift of the binding energy of the main C1s peak from 288.1 eV to 284.7 eV indicated that the supported g-C_3N_4 had higher Lewis basicity than that of the bulk g-C_3N_4. The UV–vis spectra confirmed the blue-shift of the supported g-C_3N_4 (Fig. 5). There were two main reasons for this change: the size effect of nanoscopic materials and the interaction between carbon nitride nanophases and the support. The presence of transition metal ion dopant caused some increase in the adsorption band at 400 nm. The chelating effects of transition metal ions modified the electronic structure of g-C_3N_4 nanophases to a certain extent, which was detected by UV–vis spectra (Fig. 5).

3.2. Catalytic activation and conversion CO_2

Table 2 lists the results of transferring CO_2 to epoxides. Transition metal ions (Zn^{2+}, Fe^{3+}, and Cd^{2+}) were doped into the supported g-C_3N_4 and performed the function of acid sites. The presence of transition metal ions showed negligible influences on porosity properties of g-C_3N_4/SBA-15 (Table 1). Acid sites promoted the adsorption of epoxides. Zn^{2+} was the most suitable promoter.

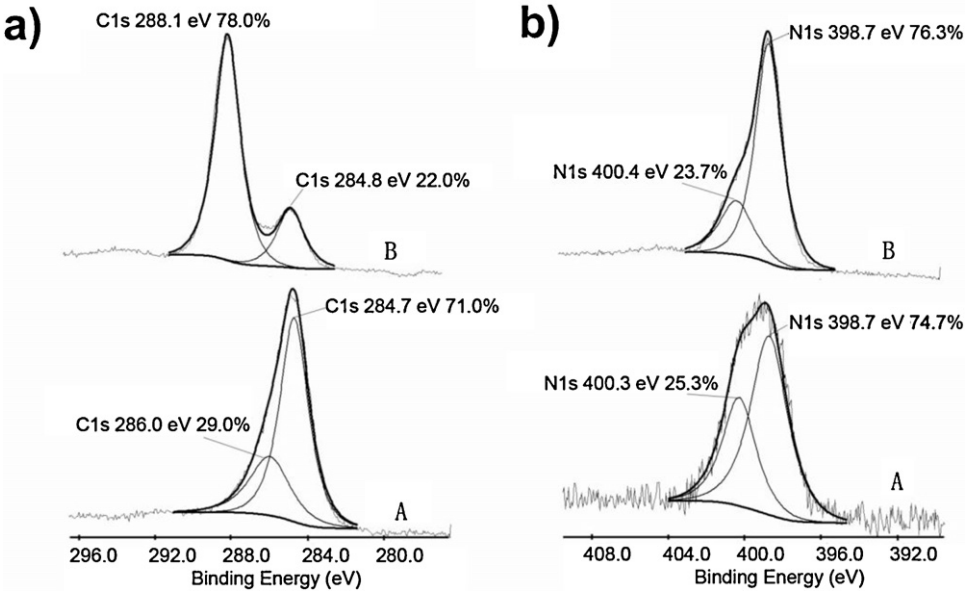

Fig. 4. (a) C1s XPS peaks of SBA-15 supported g-C_3N_4 (A) and bulk g-C_3N_4. (b) N1s XPS peaks of SBA-15 supported g-C_3N_4 (A) and bulk g-C_3N_4.

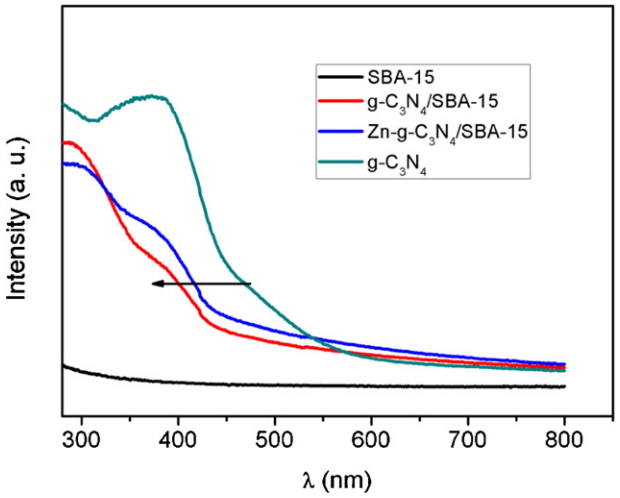

Fig. 5. UV–vis spectra of four typical samples: SBA-15, bulk g-C_3N_4, g-C_3N_4/SBA-15, Zn-doped g-C_3N_4/SBA-15.

Table 2
Experimental results of transferring the activated CO_2 to epoxides.[a]

Samples	Doped ions (wt%)	Epoxides	Conversion (%)	Selectivity (%)
SBA-15	–	Styrene oxide	0	0
g-C_3N_4/SBA-15	–	Styrene oxide	28.8	>99
SBA-15	Zn^{2+} (0.8)	Styrene oxide	7.4	79
g-C_3N_4/SBA-15	Zn^{2+} (0.8)	Styrene oxide	94.5	>99
g-C_3N_4/SBA-15[b]	Zn^{2+} (0.8)	Styrene oxide	51.7	92
Porous g-C_3N_4[c]	Zn^{2+} (0.8)	Styrene oxide	40.2	94
g-C_3N_4	Zn^{2+} (0.8)	Styrene oxide	14.1	90
g-C_3N_4/SBA-15	Cd^{2+} (0.81)	Styrene oxide	36.7	>99
g-C_3N_4/SBA-15	Fe^{3+} (0.82)	Styrene oxide	91.2	>99
g-C_3N_4/SBA-15	Zn^{2+} (0.8)	Propylene oxide	97.1	>99
g-C_3N_4/SBA-15	Zn^{2+} (0.8)	Ethylene oxide	98.3	>99

[a] Reaction conditions: epoxides: 3.0 ml, reaction temperature: 150 °C, CO_2 pressure: 3.5 MPa, reaction time: 1.5 h, catalyst amount: 0.1 g.
[b] The sample was prepared by the incipient wet impregnation of the precursors.
[c] SBA-15 was used the hard template and the silica structures were removed by HF aqueous solution.

The conversion of styrene oxide over the Zn^{2+}-doped catalyst was 94.5%, but the conversion over the blank catalyst was only 28.8%. Over Zn^{2+}-doped SBA-15, the epoxide conversion was 7.4%. The conversion of styrene oxide was 94.5% under the nonsolvent condition and the selectivity to 4-phenyl-1, 3-dioxolan-2-one was >99% after 1.5 hour reaction at 150 °C. When 1, 4-dioxane or toluene was used as the solvent, the conversion of styrene oxide was >99.9% and the selectivity toward 4-phenyl-1, 3-dioxolan-2-one was >99.5%. Under the same reaction conditions, the conversion of styrene oxide over Zn^{2+}-doped bulk g-C_3N_4 was 14.1%. Carbon nitrides over SBA-15, prepared by the incipient wet impregnation, showed the epoxide conversion of 51.7%. Porous g-C_3N_4 from the SBA-15 template converted 40.2% of the epoxide.

The Park's group has reported the possibility of the activation of CO_2 and coupling to cycloaddition [55]. In our experiments, CO_2 was used as a mild oxidant for selectively epoxidizing olefins over g-C_3N_4 nanophases in silica nanochannels. Styrene was directly converted into 4-phenyl-1, 3-dioxolan-2-one with the conversion of 10.3% after 5-h reaction at 150 °C under 3.5 MPa of CO_2 (Table 3). There is a selectivity of 91% toward the target product. Doped metal ions (Fe^{3+}, Co^{2+}, Cr^{3+}, Mn^{2+}), increased the activity. Fe^{3+}-doped g-C_3N_4/SBA-15 was the most efficient catalyst. The

Table 3
Direct oxidative cycloadditon of CO_2 to olefins.[a]

Samples	Doped ions (wt%)	Olefins	Conversion (%)	Selectivity (%)
SBA-15	–	Styrene	0	0
g-C_3N_4/SBA-15	–	Styrene	10.3	91
SBA-15	Fe^{3+} (0.82)	Styrene	0	0
g-C_3N_4/SBA-15	Fe^{3+} (0.82)	Styrene	34.1	93
g-C_3N_4/SBA-15[b]	Fe^{3+} (0.82)	Styrene	13.2	84
Porous g-C_3N_4[c]	Fe^{3+} (0.82)	Styrene	0	0
g-C_3N_4	Fe^{3+} (0.82)	Styrene	4.5	90
g-C_3N_4/SBA-15	Co^{2+} (0.82)	Styrene	24.2	94
g-C_3N_4/SBA-15	Cr^{3+} (0.81)	Styrene	13.5	95
g-C_3N_4/SBA-15	Mn^{2+} (0.82)	Styrene	26.4	92
g-C_3N_4/SBA-15	Fe^{3+} (0.82)	n-Hexene	31.6	90

[a] Reaction conditions: olefin: 3.0 mmol, 1,4-dioxane: 3.0 ml, reaction temperature: 150 °C, CO_2 pressure: 3.5 MPa, reaction time: 5 h, catalyst amount: 0.1 g.
[b] The sample was prepared by the incipient wet impregnation of the precursors.
[c] SBA-15 was used the hard template and the silica structures were removed by HF aqueous solution.

Table 4
Oxygen-aided oxidative cycloadditon of CO_2 to olefins.[a]

Samples	Doped ions (wt%)	Olefins	Conversion (%)	Selectivity (%)
g-C_3N_4/SBA-15	–	Styrene	22.3	48
g-C_3N_4/SBA-15	Fe^{3+} (0.82)	Styrene	47.5	54
g-C_3N_4/SBA-15	Co^{2+} (0.82)	Styrene	30.6	52
g-C_3N_4/SBA-15	Cr^{3+} (0.81)	Styrene	28.3	57
g-C_3N_4/SBA-15	Mn^{2+} (0.82)	Styrene	44.7	49
g-C_3N_4/SBA-15	Fe^{3+} (0.82)	n-Hexene	45.2	53

[a] Reaction conditions: olefin: 3.0 mmol, 1,4-dioxane:3.0 ml, reaction temperature: 150 °C, CO_2 pressure: 3.0 MPa, oxygen pressure: 0.5 MPa, reaction time: 5 h, catalyst amount: 0.1 g.

styrene conversion was 34.1% and the selectivity toward 4-phenyl-1, 3-dioxolan-2-one was 93%. Hexene reacted with CO_2 through the direct oxidative cycloadditon with the conversion of 31.6%. Carbon nitrides over SBA-15, prepared by the incipient wet impregnation, only converted 13.2% of styrene. Porous g-C_3N_4 from SBA-15 template showed no activity. Bulk g-C_3N_4 was a poor catalyst for the direct cycloaddition of CO_2 to styrene.

The reaction mechanism included two sequent steps: the epoxidization of styrene by CO_2 and the sequent cycloaddition of CO_2 to the epoxide. Both reactions were promoted by the doped Fe^{3+}. When molecular oxygen was introduced as the oxidant, the conversion of styrene increased, but the selectivity toward 4-phenyl-1, 3-dioxolan-2-one dropped sharply (Table 4). The involvement of oxygen in the epoxidization of styrene complicated the reaction process and decreased the selectivity to the target products. When carbon dioxide was used as oxidant, the formation of carbon monoxide was theoretically inevitable [38]. A model reaction was performed to confirm its formation. Rh^{3+}-doped g-C_3N_4/SBA-15 was selected as the catalyst for oxidative cycloaddtion of CO_2 into styrene. Rh species can catalyze the carbonylation of the resulting epoxide with the generated CO. In the final reaction mixture, a carbonylation product (3-phenyloxetan-2-one) was detected, which was the direct evidence of CO formation.

The recyclability of transition-metal-ion-doped g-C_3N_4/SBA-15 was investigated by a five-run test (Fig. 6). Three model reactions were selected: transferring CO_2 to epoxide, directly oxidative cycloaddition of CO_2 to olefins, and O_2-aided oxidative cycloaddition of CO_2 to olefins. After each run, there was a gradual decrease in the catalytic activity of Zn-g-C_3N_4/SBA-15 catalyzed cycloaddition of CO_2 to epoxides. Fig. 7 shows TEM images of the fresh catalyst and the used catalyst after the five-run recycling test of Zn-g-C_3N_4/SBA-15 for the cycloaddition of CO_2 to epoxides. The

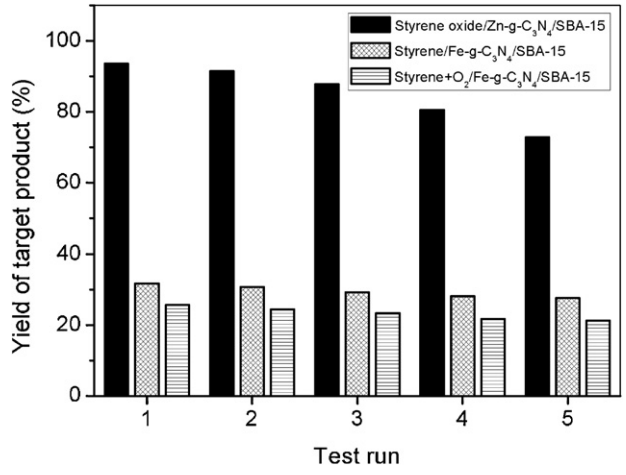

Fig. 6. Five-run recycling test of the catalysts.

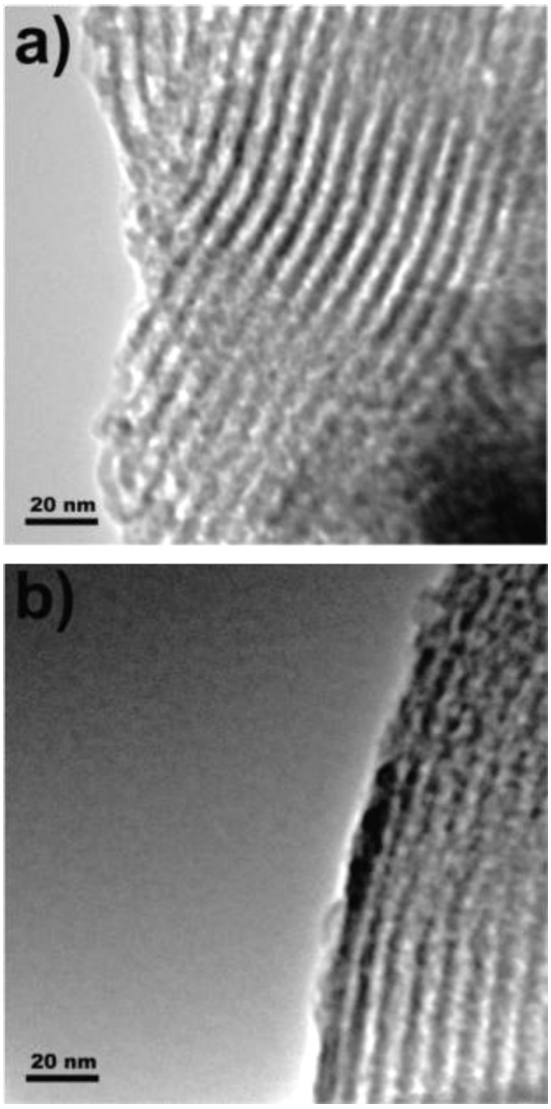

Fig. 7. (a) TEM image of g-C_3N_4/SBA-15. (b) TEM image of the used sample of Zn-g-C_3N_4/SBA-15.

mesostructures of the catalysts were kept constant and g-C_3N_4 nanophases were kept in a well-dispersed state during the catalytic process. The leaching of metal species from solid catalysts in the recycling test was detected by measuring the concentration of metal ions in the final reaction media. There was no serious metal leaching during the catalytic conversion.

3.3. The correlation between catalytic performances and microstructures of the catalyst

As revealed by Tables 2 and 3, g-C_3N_4/SBA-15, prepared by the two-step vapor condensation, exhibits higher catalytic activity for CO_2 conversion than other micro-structured g-C_3N_4 materials. Edge defects are key active sites in defect-containing polymeric C_3N_4 for CO_2 activation and conversion (Scheme 2). These low-coordinated sites have many partially-condensed nitrogen atoms, which are strong electronic donors to induce the CO_2 activation and the formation of metal ion chelates. The proportion of these edge defects is important for the catalytic activity. Well-dispersed g-C_3N_4 nanophases have more exposed edge defects than bulk g-C_3N_4. This leads to sharp increases in their catalytic activity. These active edge defects may be degraded during the preparation

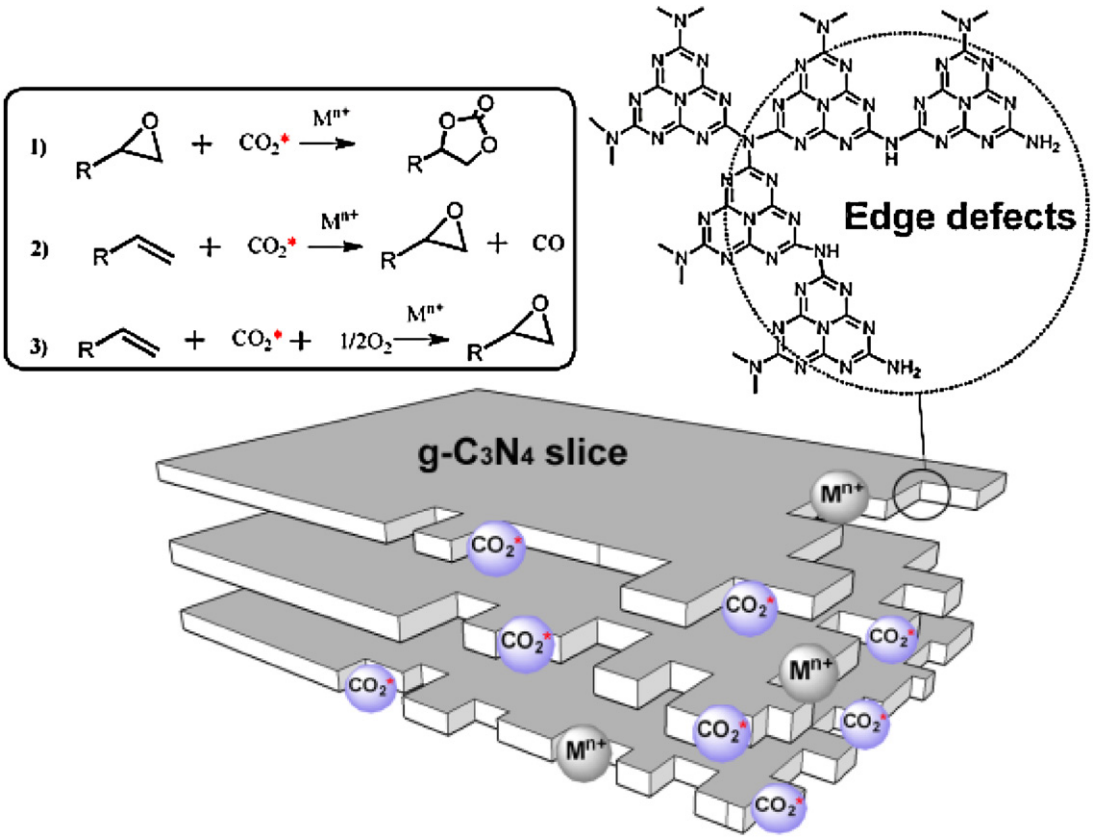

Scheme 2. Schematic illustration of catalytic active sites for CO_2 activation and conversion.

procedure. Spported carbon nitrides tolerate water molecule to a low degree (about 5% of the substrate). When carbon nitride over SBA-15 was prepared by the incipient wet impregnation, the residual water in the pore system deactivated edge defects during the high-temperature condensation. Porous g-C_3N_4 was prepared by removing SBA-15 silica templates through HF solution leaching. Such harsh treatment damaged most of edge defects. These materials showed no activity in the directly oxidative cycloaddition of CO_2 to styrene.

Quantitative analysis of the dispersion state of supported g-C_3N_4 nanophases is performed by Kerkhof–Moulijn model analysis of the XPS intensity ratio of the supports to the supported materials. Graphitic-C_3N_4 nanophases over SBA-15 can be described as a series of slabs supporting well-dispersed phase particles (Scheme 3), which is the original catalyst model proposed by Kerkhof and Moulijn [56]. This slab model assumes that the electrons leave the sample in the direction perpendicular to the surface and the emission angle (Θ) is 0°. The XPS intensity ratio of the supported phases (p) to the support (s) is formulated by:

$$\frac{I_p}{I_s} = \left(\frac{p}{s}\right)_b \frac{\sigma_p}{\sigma_s} \frac{\beta}{2} \frac{(1+e^{-\beta_1})}{(1-e^{-\beta_2})} \frac{(1-e^{-\alpha_1})}{\alpha_1} \quad (1)$$

where $(p/s)_b$ is the bulk atomic concentration, σ_p/σ_s is the relative photoelectron cross section, β is the dimensionless support thickness parameter, α is the dimensionless particle size parameter. β and α was defined as:

$$\beta_1 = \frac{t}{\lambda_{ss}}, \quad \beta_2 = \frac{t}{\lambda_{ps}}, \quad \alpha_1 = \frac{d}{\lambda_{pp}} \quad (2)$$

where t is the thickness of the support slabs, λ is the escaping depth of the electrons. The slab thickness can be estimated from the support density (ρ_s) and its surface area (S) ($t = 2/\rho_s S$). With Eq. (1), the relation between the XPS intensity ration and the dimensionless particle size parameter is given by:

$$\frac{I_p}{I_s} = Z\frac{(1-e^{-\alpha_1})}{\alpha_1} \quad (3)$$

where Z is a constant related to basic physical properties of the supported phases (p) and the support (s). α_1 is a direct index to the dispersion state of the supported phases.

With Eq. (3), the dispersion state of g-C_3N_4 nanophases are quantitated by the XPS intensity ratio of signals from g-C_3N_4 nanophases (I_{N1s}) and silica (I_{Si2p}). Four samples with different dispersion states of carbon nitrides were prepared and used as model catalysts to investigate the correlation between carbon

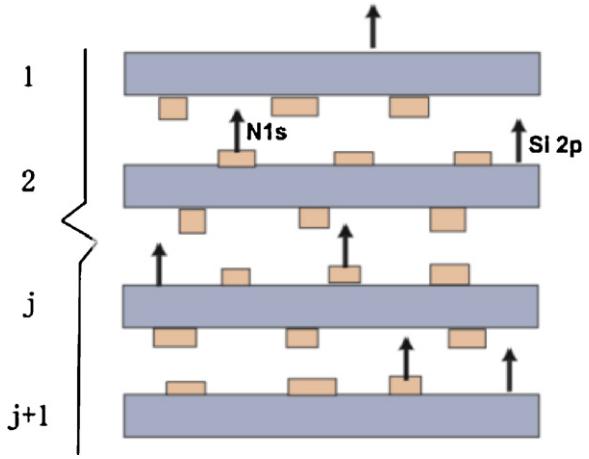

Scheme 3. Model for quantitative analysis of dispersion state of supported g-C_3N_4 nanophases.

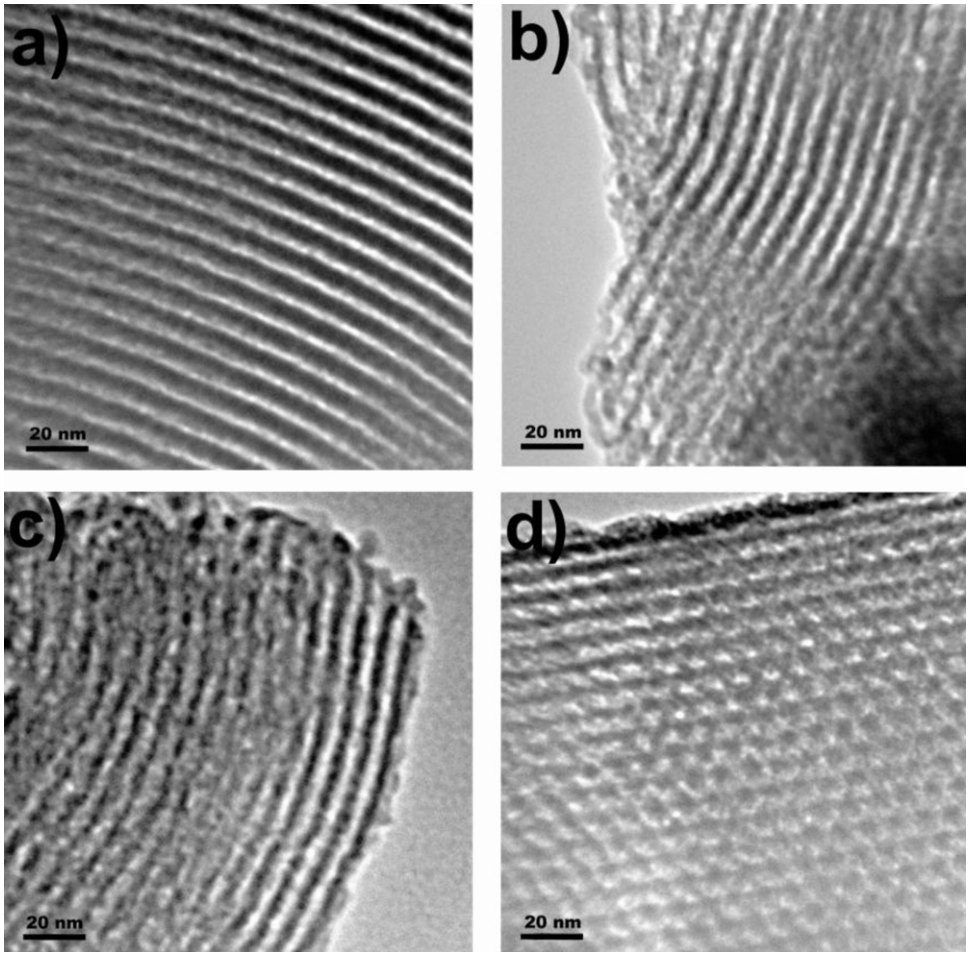

Fig. 8. (a)–(d) TEM images of the samples with different dispersion states of g-C_3N_4 nanophases over SBA-15.

nitride nanophases' dispersion and their catalytic performance. Fig. 8(a)–(d) are TEM images of the model catalysts. The dispersion states of carbon nitride nanophases are clearly discriminated. From the sample a to the sample b, the agglomeration of g-C_3N_4 nanophases are observed. The corresponding I_{N1s}/I_{Si2p} values were calculated and plotted. As shown in Fig. 9a, I_{N1s}/I_{Si2p} decreases with the increase in the degree of g-C_3N_4 agglomeration. In Fe-g-C_3N_4/SBA-15 catalyzed oxidative cycloaddition of CO_2 to styrene, the catalytic activity exhibits little fluctuation when g-C_3N_4 nanophases are kept in the well-dispersed state. But when the agglomeration of g-C_3N_4 nanophases is further aggravated, a sharp decrease in their catalytic activity is observed (Fig. 9b). The agglomeration of dispersed phases blocks the pore system of the support and leads to a decrease in the catalytic active surface.

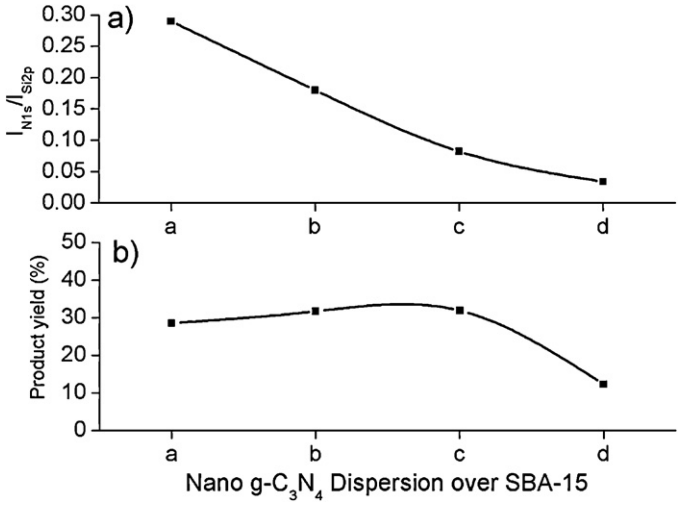

Fig. 9. (a) XPS intensity ratio of Fe-doped g-C_3N_4 to silica support (I_{N1s}/I_{Si2p}) of the samples Fig. 7(a) and (b). (b) The catalytic activity of the Fe-doped samples Fig. 7(a) and (b) for direct oxidative cycloaddition of CO_2 to styrene.

4. Conclusion

In summary, we have demonstrated that SBA-15 supported g-C_3N_4 nanophases were active catalysts for CO_2 activation and conversion. Well-dispersed g-C_3N_4 nanophases were prepared by the vapor-phase condensation of dicyandiamide in SBA-15 mesochannels. These nanostructures exhibited improved electronic properties and higher Lewis basicity than that of the bulk materials. CO_2 was activated over g-C_3N_4 nanophases and directly used as green sources of soft oxidants and carbamates. Zn^{2+}-doped g-C_3N_4/SBA-15 had a very high activity in transferring activated CO_2 to epoxides. The conversion of styrene oxide was 94.5% under nonsolvent conditions and the selectivity toward 4-phenyl-1, 3-dioxolan-2-one was >99% after the 1.5-hour reaction at 150 °C. Fe^{3+}-doped g-C_3N_4/SBA-15 was an efficient catalyst for the direct oxidative cycloadditon of CO_2 to olefins. The styrene conversion was 34.1% and the selectivity toward 4-phenyl-1, 3-dioxolan-2-one was 93%. The mesostructures of the catalysts were kept constant

during the catalytic process and g-C_3N_4 nanophases were kept in a well-dispersed state.

Acknowledgement

This work was financially supported by the National Natural Sciences Foundation of China (nos. 21174148, 21101161).

References

[1] OECD Factbook 2009: Economic, Environmental and Social Statistics, OECD, 2009.
[2] R.A. Feely, C.L. Sabine, K. Lee, W. Berelson, J. Kleypas, V.J. Fabry, F.J. Millero, Science 305 (2004) 362–366.
[3] C. Turley, Mineralogical Magazine 72 (2008) 359–362.
[4] C. Langdon, T. Takahashi, C. Sweeny, D. Chipman, J. Goddard, F. Marubini, H. Aceves, H. Barnett, M.J. Atkinson, Global Biogeochemical Cycles 14 (2000) 639–654.
[5] J.A. Kleypas, R.A. Feely, V.J. Fabry, C. Langdon, C.L. Sabine, L.L. Robbins, Impacts of Ocean Acidification on Coral Reefs and Other Marine Calcifiers, NOAA, NSF and USGS, St. Petersburg, Florida, USA, 2006.
[6] R.E. Hester, R.M. Harrison, Carbon Capture Sequestration and Storage, The Royal Society of Chemistry, Cambridge, 2010.
[7] M. Aresta, Carbon, Dioxide as Chemical Feedstock, WILEY-VCH, Weinheim, 2010.
[8] M. Aresta, Carbon Dioxide Recovery and Utilization, Kluwer, Dordrecht, 2003.
[9] A. Behr, Carbon Dioxide Activation by Metal Complexes, VCH, Weinheim, 1988.
[10] A. Behr, Angewandte Homogene Katalyse, Wiley-VCH, Weinheim, 2008.
[11] M. Aresta, W.B. Tolman (Eds.), Activation of Small Molecules, Wiley-VCH, Weinheim, 2006, pp. 1–41.
[12] T. Sakakura, J.C. Choi, H. Yasuda, Chemical Reviews 107 (2007) 2365–2387.
[13] D.J. Darensbourg, Chemical Reviews 107 (2007) 2388–2410.
[14] K. Kocía, K. Mateju, L. Obalová, S. Krejcíková, Z. Lacny, D. Plachá, L. Capekc, A. Hospodkovád, O. Solcová, Applied Catalysis B 96 (2010) 239–244.
[15] Q. Zhang, T. Gao, J.M. Andino, Y. Li, Applied Catalysis B 123–124 (2012) 257–264.
[16] Y.P. Peng, Y.T. Yeh, S.I. Shah, C.P. Huang, Applied Catalysis B 123–124 (2012) 414–423.
[17] A. Karelovic, P. Ruiz, Applied Catalysis B 113–114 (2012) 237–249.
[18] V. Jiméneza, C. Jiménez-Borjaa, P. Sáncheza, A. Romerob, E.I. Papaioannouc, D. Theleritis, S. Souentiec, S. Brosdac, J.L. Valverdea, Applied Catalysis B 107 (2011) 210–220.
[19] X. Zhong, F. Dehghani, Applied Catalysis B 98 (2010) 101–111.
[20] J.K. Leea, Y.J. Kima, Y.S. Choia, H. Leeb, J.S. Leea, J. Hongc, E.K. Jeongc, H.S. Kima, M. Cheonga, Applied Catalysis B 111–112 (2012) 621–627.
[21] M.B. Ansari, S.E. Park, Energy and Environmental Science 5 (2012) 9419–9437.
[22] M. Aresta, E. Quaranta, Proceedings of International Conference on Carbon Dioxide Utilization, Bari, 1993, pp. 63–77.
[23] D.B. Dell'Amico, F. Calderazzo, L. Labella, F. Marchetti, G. Pampaloni, Chemical Reviews 103 (2003) 3857–3897.
[24] J. Notni, S. Schenk, H. Gorls, H. Breitzke, E. Anders, Inorganic Chemistry 47 (2008) 1382–1390.
[25] B. Verdejo, J. Aguilar, E. Garcia-Espana, P. Gavina, J. Latorre, C. Soriano, J.M. Linares, A. Domenech, Inorganic Chemistry 45 (2006) 3803–3815.
[26] A. Thomas, A. Fischer, F. Goettmann, M. Antonietti, J.O. Müller, R. Schlögl, J.M. Carlsson, Journal of Materials Chemistry 18 (2008) 4893–4908.
[27] P. Dibandjo, L. Bois, F. Chassagneux, D. Cornu, J.M. Letoffe, B. Toury, F. Babonneau, P. Miele, Advanced Materials 17 (2005) 571–574.
[28] A.Y. Liu, M.L. Cohen, Science 245 (1989) 841–842.
[29] E. Kroke, M. Schwarz, Coordination Chemistry Reviews 248 (2004) 493–532.
[30] V.N. Khabashesku, J.L. Zimmerman, J.L. Margrave, Chemistry of Materials 12 (2000) 3264–3270.
[31] M. Kim, S. Hwang, J.S. Yu, Journal of Materials Chemistry 17 (2007) 1656–1659.
[32] M.H.V. Huynh, M.A. Hiskey, J.G. Archuleta, E.L. Roemer, Angewandte Chemie International Edition 44 (2006) 737–739.
[33] Y. Zhang, T. Mori, J. Ye, Science of Advanced Materials 4 (2012) 282–291.
[34] Y. Wang, J. Zhang, X. Wang, M. Antonietti, H. Li, Angewandte Chemie International Edition 49 (2010) 3356–3359.
[35] F. Goettmann, A. Fischer, M. Antonietti, A. Thomas, Angewandte Chemie International Edition 45 (2006) 4467–4471.
[36] F. Goettmann, A. Thomas, M. Antonietti, Angewandte Chemie International Edition 46 (2007) 2717–2720.
[37] X. Jin, V.V. Balasubramanian, S.T. Selvan, D.P. Sawant, M.A. Chari, G.Q. Lu, A. Vinu, Angewandte Chemie International Edition 48 (2009) 7884–7887.
[38] J. Zhang, X. Chen, K. Takanabe, K. Maeda, K. Domen, J.D. Epping, X. Fu, M. Antonietti, X. Wang, Angewandte Chemie International Edition 49 (2010) 441–444.
[39] Y. Zhang, T. Mori, J. Ye, M. Antonietti, Journal of the American Chemical Society 132 (2010) 6294–6295.
[40] Y. Zhang, A. Thomas, M. Antonietti, X. Wang, Journal of the American Chemical Society 131 (2009) 50–51.
[41] H.L. Chang, C.M. Hsu, C.T. Kuo, Applied Physics Letters 80 (2002) 4638–4640.
[42] X. Chen, J. Zhang, X. Fu, M. Antonietti, X. Wang, Journal of the American Chemical Society 131 (2009) 11658–11659.
[43] A. Vinu, K. Ariga, T. Mori, T. Nakanishi, S. Hishita, D. Golberg, Y. Bando, Advanced Materials 17 (2005) 1648–1652.
[44] Y. Jun, W. Hong, M. Antonietti, A. Thomas, Advanced Materials 21 (2009) 4270–4274.
[45] J.P. Paraknowitsch, J. Zhang, D. Su, A. Thomas, M. Antonietti, Advanced Materials 22 (2010) 87–92.
[46] F. Goettmann, A. Fischer, A. Thomas, M. Antonietti, Angewandte Chemie International Edition 45 (2006) 4467–4471.
[47] J.R. Holst, E.G. Gillan, Journal of the American Chemical Society 130 (2008) 7373–7379.
[48] Y. Zhao, J.l. Feng, Q.S. Huo, N. Melosh, G.H. Fredrickson, B.F. Chmelka, G.D. Stucky, Science 279 (1998) 548–552.
[49] M.J. Bojdys, J.O. Müller, M. Antonietti, A. Thomas, Chemistry: A European Journal 14 (2008) 8177–8182.
[50] B. Jürgens, E. Irran, J. Senker, P. Kroll, H. Müller, W. Schnick, Journal of the American Chemical Society 125 (2003) 10208–10300.
[51] B.V. Lotsch, W. Schnick, Chemistry: A European Journal 13 (2007) 4956–4968.
[52] T. Komatsu, Journal of Materials Chemistry 11 (2001) 799–801.
[53] T. Komatsu, Journal of Materials Chemistry 11 (2001) 802–805.
[54] K.S.W. Sing, D.H. Everett, R.A.W. Haul, L. Moscou, R. Pierotti, J. Rouquerol, T. Siemienwska, Pure Applied Chemistry 57 (1985) 603–619.
[55] M.B. Ansari, B.H. Min, Y.H. Mo, S.E. Park, Green Chemistry 13 (2011) 1416–1421.
[56] F.P.J.M. Kerkhof, J.A. Moulijn, The Journal of Physical Chemistry 83 (1979) 1612–1619.